Robust Reliability of Diagnostic Multi-Hypothesis Algorithms: Application to Rotating Machinery

Susanne Seibold *
Institut für Techno- und Wirtschaftsmathematik
Erwin-Schrödingerstrasse
D-67663 Kaiserslautern, Germany
seibold@itwm.uni-kl.de

Yakov Ben-Haim
Faculty of Mechanical Engineering
Technion - Israel Institute of Technology
Haifa, Israel 32000
yakov@aluf.technion.ac.il

Abstract

Damage diagnosis based on a bank of Kalman filters, each one conditioned on a specific hypothesized system condition, is a well recognized and powerful diagnostic tool. This multi-hypothesis approach can be applied to a wide range of damage conditions. In this paper, we will focus on the diagnosis of cracks in rotating machinery. The question we address is: how to optimize the multi-hypothesis algorithm with respect to the uncertainty of the spatial form and location of cracks and their resulting dynamic effects. First, we formulate a measure of the reliability of the diagnostic algorithm, and then we discuss modifications of the diagnostic algorithm for the maximization of the reliability. The reliability of a diagnostic algorithm is measured by the amount of uncertainty consistent with no-failure of the diagnosis. Uncertainty is quantitatively represented with convex models.

Keywords

Robust reliability, convex models, Kalman filtering, multi-hypothesis diagnosis, rotating machinery, crack diagnosis

1. Introduction

The diagnosis of damage in turbo-machinery is essential in the reliable, safe and economical operation of power plants, turbo-engines, and other similar equipment. Fault diagnosis is essential for early warning of incipient failure to prevent serious damage or injury, and to enable preventive maintenance or replacement. Of primary interest is the detection of damage in the machinery and the detection of large transient torsional loads.

In this paper we are primarily concerned with developing a procedure for optimizing the diagnosis of turbo-machinery with respect to the uncertain spatial form and location of cracks in a rotor shaft and their dynamic effects. In practice only very limited information is available, and for many reasons it is never possible to model the effects of a crack in the rotor shaft with complete accuracy. A crack may develop in a multitude of different ways, and its geometry will usually only be known after the shaft is cracked completely, a situation which of course should be avoided. Furthermore, most of the time plastic deformations will develop, which may have severe effects concerning the crack growth and the resulting dynamic behavior. Therefore, we will use convex models to characterize these uncertainties, rather than probabilistic models, since convex models require only sparse prior information.

* Corresponding author

We formulate a measure of the reliability of the diagnostic algorithm, and then we discuss the possible modifications of the diagnostic algorithm to maximize the reliability. We measure the reliability of a diagnostic algorithm by the amount of uncertainty consistent with no-failure of the diagnosis. A reliable algorithm will perform satisfactorily in the presence of great uncertainty. Such an algorithm is robust with respect to uncertainty, and hence the name robust reliability. On the other hand, an algorithm has low reliability when small fluctuations can lead to failure of the diagnostic decision. In this case the algorithm is fragile with respect to uncertainty.

The basic ideas underlying the different methods will be concisely described. The main contribution is to demonstrate the feasibility of combining ideas and methods from different fields as for instance multi-hypothesis diagnosis based on a model of the damage, and robust reliability.

Section 2 briefly introduces existing methods for rotor diagnosis. Section 3 outlines the concept of robust reliability and convex modeling. Section 4 describes the dynamic model of a cracked rotating shaft and section 5 outlines the design of Kalman filters for diagnosing these cracks. Section 6 extends section 4 to represent the dynamic loads of the uncertain cracks. Finally section 7 combines all the previous sections and presents the main result of the paper, which is the evaluation of the robust reliability of multi-hypothesis Kalman filters for diagnosing cracks with uncertain shape in rotors. Section 8 describes an example and section 9 discusses the interpretation of robust reliability in terms of intuitive engineering judgment.

2. Diagnosis of Rotating Machinery

Modern Machinery is bound to fulfill increasing demands concerning durability and safety requirements. In order to avoid severe damage, powerful tools for the monitoring and diagnosis have to be developed. Current trends are described e.g. by *Williams and Davies (1992).* The diagnosis of turbomachinery is of particular relevance, in order to avoid catastrophic damage or injury, *Haas (1977), Muszynska (1992).*

Of primary interest is the detection of cracks in rotor shafts. *Wauer (1990)* gives a concise overview about the research performed in the area of modeling the dynamics of a cracked rotor and detection procedures. A crack in a rotor shaft influences the rotor vibrations, especially the first, second and third harmonic. Besides, a shifting of the phase occurs. Therefore, a suitable analysis of the measurement signals yields valuable hints for the detection of a crack. But it is impossible to diagnose the size of the damage or its location based on mere signal analysis.

Increasingly, model-based procedures are developed which aim at closing this gap by establishing an algorithmic relation between the measurements and a suitable model of the system. In this way, the redundancy between model and measurements can be employed to determine the size and location of a damage. Many of these tools have been developed in the field of control theory, *Frank (1990), Isermann (1984), Willsky (1976),* and can be successfully applied to the diagnosis of cracks in rotating systems, *Seibold (1995), Seibold and Weinert (1996).* Model-based diagnosis can be performed by a variety of procedures, which are classified into two groups, *Frank (1990), Isermann (1984), Willsky (1976)*: observer-based procedures, like for instance parity space approach, bank of observers or filters, innovations tests and failure sensitive filters, and parameter identification procedures, like for instance Least Squares, Instrumental Variables, Maximum Likelihood and Extended Kalman Filter as state and parameter estimator. In fact, these two groups are interrelated.

In this paper, the aim is to investigate the reliability of such a model-based diagnostic algorithm for the special case of localizing cracks in rotor shafts while considering the uncertainties in the model of the crack.

3. Robust Reliability and Convex Sets

The reliability of a system is a measure of its resistance to uncertainties. Uncertainties arise in many different ways: the mechanical model itself may be uncertain, or the loads acting on the system may not be completely known or measurable. The uncertain phenomena may be constant or varying with time. For example, it is hardly ever possible to model every phenomenon that may occur. Furthermore, it may not always be desirable to work with a large-dimensional model. Rather, one tries to reduce the model size, while retaining the relevant dynamic effects. This of course may yield additional uncertainties which have to be taken into account.

The concept of robust reliability (as opposed to probabilistic reliability) used in this paper is that a system is reliable if it can tolerate large amounts of uncertainty without failing, *Ben-Haim (1995, 1996, 1997)*. On the other hand, it is unreliable if even small deviations from the nominal circumstances can lead to failure. In analogy, it is possible to formulate a measure for the robustness of a diagnostic algorithm. A reliable algorithm will perform satisfactorily in the presence of great uncertainties. Such an algorithm is robust with respect to uncertainty, and hence the name robust reliability. On the contrary, an algorithm has low reliability if even small fluctuations can lead to failure of the diagnosis. In this case the algorithm is fragile with respect to uncertainty.

Robust reliability analysis consists of three components, *Ben-Haim (1996)*:

- A **mechanical model** of the system,
- a **failure criterion** specifying the conditions which constitute failure of the system or of the diagnostic algorithm,
- and an **uncertainty model**, quantifying the uncertainties to which the system is subjected. These uncertainties may appear in the mechanical model and the loads as well as in the failure criterion.

Classical probability theory relies on the frequency of occurrence of events to model the uncertainty. However, in many applications there is only limited information available. It may not be possible to perform enough tests and measurements to cover the whole spectrum of possible input-output behavior. Furthermore, the rare events may be the most dangerous ones regarding the remaining life time of the system, and relevant frequency data may be very sparse or lacking. On the contrary, set-theoretical models of uncertainty describe how the uncertain events cluster, and the size of the set indicates how much uncertainty is anticipated. A convex model is a nested family of sets, $U(\alpha)$ for $\alpha \geq 0$, which expand like a balloon as the uncertainty parameter grows. Convex models of uncertainty are always based on a-priori information about the uncertain events, but they require less information than probabilistic models. Convex models are discussed in *Ben-Haim (1985, 1994, 1996)* and *Ben-Haim and Elishakoff (1990)*.

Employing convex sets, it is possible to measure the uncertainty with a specific uncertainty parameter α, which may also be called the expansion parameter of the convex set, *Ben-Haim (1985)*. A convex set $U(\alpha)$ will change its size according to the changing of α, while the shape is retained, much like a balloon expands and contracts. The main goal of a robust reliability analysis is to determine how large the uncertainty parameter α can become before the system can fail.

4. Modeling a Crack in a Rotating Shaft

Numerous concepts for the modeling of cracks in rotating shafts have been developed, *Wauer (1990)*. The first models were based on the assumption of a simple Jeffcott-rotor with a breathing crack, and already incorporated the relevant dynamic effects, see e.g. *Gasch (1976)*. "Breathing" here means that the crack will open and close during the rotation of the shaft, depending on the actual displacements. Later, finite beam elements with a breathing crack were developed, which can be applied to the diagnosis of large turbine shafts. *Theis (1990)* has developed such a crack model which takes into account all six degrees of freedom of the Bernoulli beam theory. In most practical cases, weight dominance can be assumed, which means that the vibration amplitudes are small compared to the static deflection due to the weight. The Theis model does not require weight dominance. But this assumption is advantageous as we will see.

Employing the small amplitude approximation, the following linear differential equations can be derived, where the additional dynamics due to the crack are modeled as "external crack loads" $\underline{F}_R$ acting on the system, *Theis (1990)*, *Seibold and Weinert (1996)*:

$$\underline{M}\,\Delta\ddot{\underline{q}}(\varphi) + \underline{D}\,\Delta\dot{\underline{q}}(\varphi) + \underline{K}_0\,\Delta\underline{q}(\varphi) = \underline{F}_R(\varphi) + \underline{F}_U(\varphi)\,, \tag{4.1}$$

$\underline{M}$ and $\underline{D}$ being the mass and damping matrices, $\underline{K}_0$ being the stiffness of the uncracked system, $\Delta\underline{q}$ being the vibrations around the static deflection, φ being the angle of rotation, $\underline{F}_U$ being the unbalance excitation, *Seibold (1995)*, and $\underline{F}_R$ being the crack loads.

In *Theis (1990)*, it is described how the additional compliance due to the crack and subsequently the vector of crack loads $\underline{F}_R$ can be derived via the energy release rate based on fracture mechanical considerations. In order to facilitate the application to model-based damage diagnosis, the crack loads can be approximated by polynomial functions, *Seibold (1995)*:

$$\underline{F}_R(a,\varphi) = \left(\sum_{i=0}^{n} a^i\,\underline{P}_i\right)\underline{\gamma}(\varphi) = \underline{R}(a)\,\underline{\gamma}(\varphi)\quad, \tag{4.2}$$

where a is the depth of the crack, $\underline{P}_i$ are constant matrices of coefficients independent of a and φ, and

$$\underline{\gamma}(\varphi)^T = \left[1\ \sin\varphi\ \sin 2\varphi \ldots \sin k\varphi\ \cos\varphi\ \cos 2\varphi \ldots \cos k\varphi\right]\,, \tag{4.3}$$

is a function of the angle of rotation φ.

5. Kalman Filter Design for the Diagnosis of Cracks

The Kalman Filter was developed by *Kalman (1960)* to estimate unknown states of linear systems based on noisy measurements. *Jazwinski (1970)* describes how the Kalman Filter can be modified for nonlinear systems. This Extended Kalman Filter (EKF) may also be used for a parallel identification of states and parameters. The EKF requires a representation of the system equations in state space, so that a state space vector $\underline{z}$ has to be defined. If mechanical systems are treated, it consists of the vectors of displacement and velocity $\underline{q}$ and $\dot{\underline{q}}$, and may be extended by the vector of unknown parameters $\underline{p}$ for the purpose of parameter identification:

$$\underline{z}^T = \left[\underline{q}^T \quad \dot{\underline{q}}^T \quad \underline{p}^T\right] . \tag{5.1}$$

Let us assume that we have modeled a rotor with a crack in the shaft according to eq. (4.1), and that we can describe the vector of crack loads $\underline{F}_R$ according to (4.2). Based on this model, an EKF can be designed to estimate the crack depth, a, based on incomplete measurements $\underline{y}$. In this case the vector $\underline{p}$ = a is a scalar.

The EKF is a recursive algorithm, so that for the first time step, initial estimates of the state space vector have to be provided. At time step k+1, the estimate of the state space vector $\underline{z}_{k+1}$ is calculated as:

$$\hat{\underline{z}}_{k+1/k} = \hat{\underline{z}}_k + \int_{t_k}^{t_{k+1}} \underline{f}(\hat{\underline{z}}_k, t_k, \underline{p}, \underline{u})\, dt = \underline{A}\ \hat{\underline{z}}_k + \underline{B}\left\{\underline{F}_U(\varphi) + \underline{F}_R(\varphi)\right\}, \tag{5.2}$$

where $\underline{u}$ are the inputs into the system. In our case, the inputs are the unbalance excitation $\underline{F}_U$, and the crack loads $\underline{F}_R(\varphi)$. Note that the parameter $\underline{p}$ =a appears only in the vector of crack loads $\underline{F}_R(\varphi)$.

The covariance matrix of the states is estimated as

$$\underline{P}_{k+1/k} = \underline{A}_k^*\ \underline{P}_k\ \underline{A}_k^{*T} + \underline{Q}_k \quad . \tag{5.3}$$

where

$$\underline{A}_k^* = \exp(\underline{F}\,\Delta t)\,,\ \underline{F} = \left(\frac{\partial \underline{f}_i(t, \underline{z}, \underline{u})}{\partial z_j}\right)\Bigg|_{\underline{z}=\underline{z}_k},\ \Delta t_k = t_{k+1} - t_k\,. \tag{5.4}$$

At each time step k, the linearized discrete system matrix $\underline{A}_k^*$ and the discrete equivalent of the covariance matrix of the system noise $\underline{Q}_k$ have to be calculated based on the current estimate of the parameter. The prediction is corrected on the basis of measurements $\underline{y}_{k+1}$:

$$\hat{\underline{z}}_{k+1} = \hat{\underline{z}}_{k+1/k} + \underline{K}_{g_{k+1}}\left\{\underline{y}_{k+1} - \underline{C}\ \hat{\underline{z}}_{k+1/k}\right\} \quad , \tag{5.5}$$

$$\underline{P}_{k+1} = \left(\underline{I} - \underline{K}_{g_{k+1}}\ \underline{C}\right)\underline{P}_{k+1/k}\left(\underline{I} - \underline{K}_{g_{k+1}}\ \underline{C}\right)^T + \underline{K}_{g_{k+1}}\ \underline{P}_{k+1/k}\ \underline{K}_{g_{k+1}}{}^T \quad , \tag{5.6}$$

$$\underline{K}_{g_{k+1}} = \underline{P}_{k+1/k}\ \underline{C}^T\left(\underline{C}\ \underline{P}_{k+1/k}\ \underline{C}^T + \underline{R}_{k+1}\right)^{-1} \quad . \tag{5.7}$$

The differences between model prediction and measurements (see eq. (5.5)), are termed innovations:

$$\underline{v}_{k+1} = \underline{y}_{k+1} - \underline{C}\,\hat{\underline{z}}_{k+1/k}\,. \tag{5.8}$$

The crack diagnosis must identify two quantities: the location and the effective (or “equivalent”) depth of the crack. In the multi-hypothesis approach we “tune” each of a bank of EKFs to a different hypothesized location of the crack. Usually, one can assume that the measurement noise is normally distributed and uncorrelated with zero mean. Then, the innovations of the EKFs are time series with the same properties **if** measurement and model prediction are corresponding. In other words, if the hypothesized crack location for a particular EKF is correct, then the innovation sequence will be normally distributed with zero mean and uncorrelated in time. These properties will not (usually) hold for an EKF where the hypothesized crack location is erroneous. Therefore, a statistical analysis of the innovations can lead to a localization of the damage. The standard deviation is a good measure, because the filter based on the “best” hypothesis will yield innovations with the least standard deviation S_i, where

$$S_i^{\,2} = \frac{1}{N}\sum_{i=1}^{N}\left(\underline{v}_i - \hat{\underline{v}}\right)\left(\underline{v}_i - \hat{\underline{v}}\right)^T \quad , \tag{5.9}$$

where $\hat{\underline{v}}$ is the mean value of the innovations. Of course, there are many more possibilities for a statistical analysis, *Mehra and Peschon (1971)*.

6. Modeling the Uncertain Crack Loads

Different cracks of the same net depth (or effective crack area) produce different crack loads due to their different crack-front shapes. This variation of the crack loads is quantified approximately, (to the best of our knowledge which is very fragmentary, because the true crack front shape can only be determined after the shaft is completely cracked) by a convex model. Let the uncertain vector of crack loads $\underline{\tilde{F}}_R$ consist of a known part R(a) according to eq. (4.2), and a part $\underline{U}$ which accounts for the crack uncertainty:

$$\underline{\tilde{F}}_R(a,\varphi) = \underline{R}(a)\,\underline{\gamma}(\varphi) + \underline{U} \quad . \tag{6.1}$$

Our prior knowledge about the crack uncertainties is used to choose a convex model for $\underline{U}$. In the face of severe lack of information we will use a very simple convex model, such as the ellipsoid-bound convex model:

$$D_1(\alpha_1) = \left\{\underline{U}: \|\underline{U}\|^2 \le {\alpha_1}^2\right\} \quad . \tag{6.2}$$

$D_1(\alpha_1)$ is the set of all uncertain load vectors $\underline{U}$ whose norm does not exceed α_1. The range of variability of $\underline{U}$ increases as the uncertainty parameter α_1 increases. However, if we have spectral information available, one might choose a fourier-ellipsoid-bound model. The temporal variation of the uncertain crack loads are expressed by a truncated Fourier-series as:

$$\underline{U} = \underline{V}\,\underline{\eta}(\varphi) \quad , \tag{6.3}$$

where $\underline{\eta}(\varphi)$ is a known vector of trigonometric functions:

$$\underline{\eta}(\varphi)^T = \left[1 \;\; \sin\varphi \;\; \sin 2\varphi \ldots \sin k\varphi \;\; \cos\varphi \;\; \cos 2\varphi \ldots \cos k\varphi\right] \quad , \tag{6.4}$$

and $\underline{V}$ is a matrix of uncertain Fourier coefficients. The uncertainty in $\underline{U}(\varphi)$ is expressed by uncertainty in the coefficient matrix $\underline{V}$. One way is to employ an ellipsoid-bound convex model for the uncertainty in $\underline{V}$:

$$D_2(\alpha_2) = \left\{\underline{V}: \|\underline{V}\|^2 \le {\alpha_2}^2\right\}. \tag{6.5}$$

We note that the uncertainty parameters α_1 and α_2 each control the "size" of the corresponding convex model: as α_i increases, the range of variability of $\underline{U}$ increases. However, the convex models D_1 and D_2 are quite different in nature. D_1 contains crack-load vectors whose rate of variation is unbounded, while D_2 contains band-limited load vectors only. In other words, even if α_1 and α_2 have the same value, the range of variation of $\underline{U}$ on D_1 and on D_2 will differ, as will, for instance, the maximum norm of $\underline{U}$.

In the approach presented here, convex models are chosen to describe the uncertainty of the model, because they fit very well to the type of information available. That does not imply that probabilistic models would not fit. However, they would require much more information than is available here.

7. Robust Reliability of a Diagnostic Multi-Hypothesis Algorithm

Damage diagnosis based on a bank of Kalman Filters, each one conditioned on the hypothesis that a crack exists at a specific location as described in section 5, is a well recognized diagnostic tool. The robust reliability of a diagnostic algorithm is measured by the amount of uncertainty consistent with no-failure of the diagnosis. A reliable algorithm will perform satisfactorily even in the presence of great uncertainty.

The aim of our diagnostic algorithm is the localization of a crack in a rotor and the determination of its "equivalent" or approximate depth. For a robust reliability analysis and a subsequent maximization of the reliability of our multi-hypothesis algorithm, we need three components as explained in section 3. The **mechanical model** of our rotor may be derived with a finite-element code, with the crack modeled according to eq. (4.2). The **uncertainty** $\underline{U}$ of the crack loads is expressed by a convex model according to eq. (6.2) or (6.5). Finally, we need to specify a **failure criterion** for our diagnostic algorithm. Intuitively, one would immediately think of two different failure criteria, one relating to the uncertain crack shape, and the other concerning the unknown crack location. In the following, these two different failure criteria will be discussed in sections 7.1 and 7.2. The two different uncertainty models (6.2) and (6.5) will both be employed.

To demonstrate the procedure, let us make an approximation and express $\underline{R}(a)$ by the linear function

$$\underline{R}(a) = a\,\underline{P}_1 + \underline{P}_0 \quad . \tag{7.1}$$

In practice one usually needs at least a cubic term, so that n=3 in eq. (4.2). If nonlinear terms are included, the maximization of the robust reliability has to be performed numerically.

7.1 Maximizing the Robust Reliability of the Crack Depth Estimate

For the maximization of the robust reliability of the crack depth estimate, we have to define an error criterion, like for instance: "The diagnostic algorithm fails if the error in the estimated crack depth is too great". Let ε denote the error of the crack-depth estimate and let ε_{CR} denote the greatest acceptable error of the estimate. Failure of the diagnosis occurs if:

$$\varepsilon \geq \varepsilon_{CR} \quad . \tag{7.2}$$

For the robust reliability analysis with respect to the diagnosis of the crack, we need to examine the recursive estimates $\hat{a}$ of the crack depth. Writing only the estimation equation for the crack depth, one has one line from the vector relation (5.5):

$$\hat{a}_{k+1} = \hat{a}_k + \underline{K}_{ag_{k+1}} \left\{ \underline{y}_{k+1} - \underline{C}\,\underline{\hat{z}}_{k+1/k} \right\} \quad , \tag{7.3}$$

where $\underline{K}_{ag}$ is the bottom row of the Kalman gain matrix $\underline{K}_g$. Taking account of the model prediction (5.2), eq. (7.3) becomes

$$\hat{a}_{k+1} = \hat{a}_k + \underline{K}_{ag_{k+1}} \left[\underline{y}_{k+1} - \underline{C} \left\{ \underline{A}\,\underline{\hat{z}}_k + \underline{B}\,\underline{F}_U(\varphi) + \underline{B}\left(\underline{R}(a)\,\underline{\gamma}(\varphi) + \underline{U} \right) \right\} \right] \quad . \tag{7.4}$$

If the estimation is successful, the Kalman gain will converge within certain bounds as well as the estimate $\hat{a}$ of the crack depth.

7.1.1 Ellipsoid-bound model of uncertainty

Let us first analyze the robust reliability for a simple ellipsoid-bound model, eq. (6.2). Expressing $\underline{R}(a)$ by (7.1), and assuming the Kalman gain and the estimates converge, eq. (7.4) becomes:

$$\hat{a} = -\frac{\underline{G}}{S_1(\varphi)}\ \underline{U} + \frac{S_2(\varphi)}{S_1(\varphi)} + \frac{S_3(\varphi)}{S_1(\varphi)}\ , \tag{7.5}$$

denoting

$$\underline{G} = \underline{K}_{ag}\ \underline{C}\ \underline{B}\ , \tag{7.6}$$

$$S_1 = \underline{G}\,\underline{P}_1\,\underline{\gamma}(\varphi)\ , \tag{7.7}$$

$$S_2 = \underline{K}_{ag}\ \underline{y}(\varphi) - \underline{K}_{ag}\ \underline{C}\left\{\underline{A}\,\underline{\hat{z}}(\varphi) + \underline{B}\,\underline{F}_U(\varphi)\right\}\ , \tag{7.8}$$

$$S_3 = -\underline{G}\,\underline{P}_0\,\underline{\gamma}(\varphi)\ . \tag{7.9}$$

Eq. (7.5) shows how the crack depth estimate varies due to the uncertainty in the crack loads $\underline{U}$. The first term on the right hand side expresses the effect of uncertain crack variability, while the other terms on the right correspond to the nominally straight crack-front shape. For the same nominal value of crack depth, a, the estimated crack depth varies over the range of values taken by $\left(\underline{G}/S_1(\varphi)\,\underline{U}\right)$ as $\underline{U}$ varies on $\mathtt{D}_1(\alpha_1)$.

If this variation of the estimate is small, then the diagnosis is robust since the crack uncertainty only weakly influences the estimate. On the other hand, if this variation is large, then the diagnosis is fragile to uncertainty and hence unreliable. To evaluate the variability of the crack depth estimate, we maximize (7.5) employing the Cauchy inequality and (6.2):

$$\max \hat{a} = \hat{a}_{nom} + \frac{\alpha_1}{|S_1(\varphi)|}\,\|\underline{G}\|_2\ , \tag{7.10}$$

where $\hat{a}_{nom}$ is the nominal estimate (the second and third terms on the right of eq. (7.5)) and $\|...\|_2$ denotes the Euclidean norm. The second term on the right results from the load uncertainty, and depends on the uncertainty parameter α_1.

The robust reliability is the greatest value of the uncertainty parameter, α_1, consistent with no-failure of the estimates. Equating $\max(\hat{a} - \hat{a}_{nom})$ to ε_{CR} and solving for α_1, we obtain the robust reliability $\breve{\alpha}_1$:

$$\max(\hat{a} - \hat{a}_{nom}) = \varepsilon_{CR} \quad \Rightarrow \quad \breve{\alpha}_1 = \frac{|S_1(\varphi)|}{\|\underline{G}\|_2}\,\varepsilon_{CR}\ . \tag{7.11}$$

When $\breve{\alpha}_1$ is large, the diagnosis is robust with respect to uncertainty. On the other hand, when $\breve{\alpha}_1$ is small, the diagnosis fails even in the presence of minor crack uncertainties. Note that if the Kalman estimate of the crack depth has converged in eq. (7.4), then the robustness $\breve{\alpha}_1$ will still vary with φ, because of the angle-dependency of the vector of trigonometric functions, $\gamma(\varphi)$.

7.1.2 Fourier-bound model of uncertainty

If the fourier-ellipsoid-bound model, eq. (6.5), is employed, a different relation between crack depth estimate and uncertainty is derived. We employ the following property of the Kronecker product

$$\mathrm{vec}\left(\underline{A}\,\underline{X}\,\underline{B}\right) = \left(\underline{B}^{T} \otimes \underline{A}\right)\mathrm{vec}\,\underline{X} \quad , \tag{7.12}$$

Lancaster and Tismenetsky (1985). vec($\underline{A}$) is the vector formed by concatenating the columns of $\underline{A}$. Then, assuming the convergence of the estimate within certain bounds, (7.4) becomes:

$$\hat{a} = \frac{\underline{S}_4(\varphi)}{S_1(\varphi)}\ \mathrm{vec}\,\underline{V} + \frac{S_2(\varphi)}{S_1(\varphi)} + \frac{S_3(\varphi)}{S_1(\varphi)} \quad , \tag{7.13}$$

where

$$\underline{S}_4 = -\left(\underline{\eta}^{T}(\varphi) \otimes \underline{G}\right) \quad . \tag{7.14}$$

Eq. (7.13) shows how the crack depth estimate varies due to the uncertainty in the crack loads, $\underline{V}$, based on the fourier-bound convex model $D_2(\alpha_2)$. Now, the error of the crack depth estimate may be as great as the maximum value attained by $\underline{S}_4(\varphi) \big/ S_1(\varphi)\,\mathrm{vec}\,\underline{V}$. We maximize (7.13) employing the Cauchy inequality and (6.5):

$$\max \hat{a} = \hat{a}_{nom} + \frac{\alpha_2}{|S_1(\varphi)|}\left\| \underline{\eta}^{T} \otimes \underline{G} \right\|_2 \quad , \tag{7.15}$$

where $\hat{a}_{nom}$ is the nominal estimate (the second and third terms on the right of eq. (7.13)). By equating $\max(\hat{a} - \hat{a}_{nom})$ to ε_{CR} and solving for α_2, we obtain the robust reliability:

$$\max(\hat{a} - \hat{a}_{nom}) = \varepsilon_{CR} \quad \Rightarrow \quad \breve{\alpha}_2 = \frac{|S_1(\varphi)|}{\left\| \underline{\eta}^{T} \otimes \underline{G} \right\|_2}\ \varepsilon_{CR} \quad . \tag{7.16}$$

At this point, it has to be stated that only robust reliability parameters derived on the basis of the same uncertainty model and failure criterion are directly comparable. However, examining (7.11) and (7.16), one can show that $\breve{\alpha}_1$ and $\breve{\alpha}_2$ only differ by the factor $\left\| \underline{\eta}^{T} \right\|_2$. If we let the fourier-bound model approach the ellipsoid-bound model by allowing $\underline{\eta}$ to become unity, (7.16) will converge to (7.11).

7.2 Maximizing the Robust Reliability of the Crack Localization

For the diagnosis of the crack location, a bank of Extended Kalman Filters (EKF) is designed, consisting of several filters, each one tuned to a specific crack location. The structure of this multi-hypothesis algorithm is a parallel one. In the context of reliability, however, the bank of filters can be regarded as a serial network. That is, the diagnostic algorithm fails if even one of the EKFs yields faulty results. Therefore, the reliability of the bank of EKFs is only as large as the reliability of the "weakest" EKF.

As described in section 5, the crack can be localized based on a bank of EKFs by evaluating the innovations generated by each of these filters. To demonstrate the robust reliability analysis, let us assume that we have only one measurement, y, so that the matrix $\underline{C}$ is a row vector. For more than one measurement the procedure is much the same, since we treat the individual innovations separately. For simplicity we consider only one measurement.

Then, the innovations generated depend on the uncertain crack loads in the following way, based on (5.8):

$$v_{k+1} = y_{k+1} - J_1 - \underline{J}_2 \, \underline{U} \quad , \tag{7.17}$$

where

$$J_1 = \underline{C}\left\{\underline{A}\,\underline{\hat{z}}_k + \underline{B}\,\underline{F}_U(\varphi) + \underline{B}\,\underline{R}(a)\,\underline{\gamma}(\varphi)\right\}, \tag{7.18}$$

and

$$\underline{J}_2 = \underline{C}\,\underline{B} \quad . \tag{7.19}$$

The statistical analysis is performed for R revolutions of the rotor, assuming m measurements per revolution. So eq. (7.17) is repeated at mR times (or angles):

$$\underbrace{\begin{bmatrix} v_1 \\ . \\ . \\ v_{mR} \end{bmatrix}}_{\underline{\tilde{v}}} = \underbrace{\begin{bmatrix} y_1 \\ . \\ . \\ y_{mR} \end{bmatrix} - \begin{bmatrix} J_1 \\ . \\ . \\ J_{mR} \end{bmatrix}}_{\underline{\tilde{v}}_{nom}} - \underline{\tilde{v}}_U \quad , \tag{7.20}$$

where $\underline{\tilde{v}}_U$ accounts for the uncertain crack loads, and "nom" is the abbreviation for the nominal innovations (the second and third terms on the right-hand side of eq. (7.17)). The "nominal" innovations result from measurement and system noise other than the crack-shape uncertainty. An equation such as (7.20) holds for each filter, though we have suppressed the filter index. The mathematical form of $\underline{\tilde{v}}_U$ depends on the convex model being used, as we will explain later in sections 7.2.1 and 7.2.2 for the two different convex models under consideration.

Each filter in the bank is "tuned" to a different crack location. The filter with the correct hypothesized crack location will have zero-mean white innovations with low variance. The other filters will not be zero-mean and will tend to have larger variance. The crack location is identified by lowest variance. The diagnostic algorithm fails if even one filter yields innovations with a similar or a smaller variance than the filter based on the correct hypothesis. On the contrary, "no-failure" of the diagnosis occurs if the variance $S^2_{correct}$ of the filter with the correct hypothesis is the smallest from the bank of filters:

$$S^2_{correct} = \min_i \frac{1}{mR} \left\| \underline{\tilde{v}}_i \right\|^2 \quad , \tag{7.21}$$

where i is the filter index. Analogous to the above, we consider two convex models of uncertainty for the robust reliability analysis.

7.2.1 Ellipsoid-bound model of uncertainty

Employing the ellipsoid-bound model of uncertainty (6.2), relation (7.20) becomes:

$$\tilde{\underline{v}} = \tilde{\underline{v}}_{nom} - \left(\underline{J}_2 \ \underline{U}\right)\tilde{\underline{I}} \quad , \tilde{\underline{I}}^T = (1,1,1,\ldots.1) , \tilde{\underline{I}} \in \Re^{mR} . \tag{7.22}$$

Squaring (7.22) yields:

$$\tilde{\underline{v}}^T \tilde{\underline{v}} = \left\|\tilde{\underline{v}}_{nom}\right\|^2 - 2\left(\underline{J}_2 \underline{U}\right)\tilde{\underline{v}}_{nom}{}^T \tilde{\underline{I}} + mR\left(\underline{J}_2 \underline{U}\right)^2 \tag{7.23}$$

For the correct hypothesis, the second term on the right hand side is asymptotically zero, because $\tilde{\underline{v}}_{nom}{}^T \tilde{\underline{I}}$ is proportional to the mean innovation. We have assumed in section 5, that for the correct hypothesis the innovations are normally distributed and uncorrelated with zero mean.

Maximizing (7.23) as $\underline{U}$ varies on $D_1(\alpha_1)$ by employing the method of Lagrange multipliers and dividing by the number of measurements mR yields the greatest variance of the innovations:

$$S^2_{max,i} = \frac{1}{mR}\left\|\tilde{\underline{v}}_{nom,i}\right\|^2 + \alpha_1{}^2 \left\|\underline{J}_2\right\|^2 . \tag{7.24}$$

The least variance of the innovations occurs when $\underline{U}$ is orthogonal to $\underline{J}_2$:

$$S^2_{min,i} = \frac{1}{mR}\left\|\tilde{\underline{v}}_{nom,i}\right\|^2 . \tag{7.25}$$

Eq. (7.21) states that the bank of EKFs succeeds in locating the crack if the filter whose innovations are least in fact corresponds to the correct crack location. This is what would happen (asymptotically) if there were no crack-shape uncertainty. Let us renumber the filters so that $\left\|\tilde{\underline{v}}_{nom,1}\right\|^2$ is the least and $\left\|\tilde{\underline{v}}_{nom,2}\right\|^2$ is the next greatest value. The bank of filters fails according to criterion (7.21), if the crack-shape uncertainty causes $S_1{}^2$ to increase and causes $S_2{}^2$ to diminish, so that the $S_1{}^2 \geq S_2{}^2$. In other words, (7.21) is equivalent to the following failure criterion: the diagnosis fails, if the **greatest** variance of the correct filter exceeds the **least** variance of the next largest filter:

$$S_{max,1}{}^2 \geq S_{min,2}{}^2 \quad . \tag{7.26}$$

Using eqs. (7.24) and (7.25), this relation becomes:

$$\frac{1}{mR}\left\|\tilde{\underline{v}}_{nom,1}\right\|^2 + \alpha_1{}^2\left\|\underline{J}_2\right\|^2 \geq \frac{1}{mR}\left\|\tilde{\underline{v}}_{nom,2}\right\|^2 \quad . \tag{7.27}$$

The least value of the uncertainty parameter α_1 at which this occurs is the robust reliability of the bank of filters:

$$\breve{\alpha}_1 = \frac{1}{\sqrt{mR}\left\|\underline{J}_2\right\|}\sqrt{\left\|\tilde{\underline{v}}_{nom,2}\right\|^2 - \left\|\tilde{\underline{v}}_{nom,1}\right\|^2} \quad . \tag{7.28}$$

The denominator in eq. (7.28) is a function of the measurement matrix $\underline{C}$. Therefore, with a suitable sensor deployment, the robust reliability of the crack localization can be maximized.

7.2.2 Fourier-bound model of uncertainty

Now, we evaluate the robust reliability based on the fourier-bound convex model (6.5). Similar to the above, taking advantage of the properties of the Kronecker product one can derive

$$\begin{aligned}\underline{\tilde{v}} &= \underline{\tilde{v}}_{nom} - \begin{bmatrix} \underline{\eta}_1{}^T \otimes \underline{J}_2 \\ \cdot \\ \cdot \\ \underline{\eta}_{Rm}{}^T \otimes \underline{J}_2 \end{bmatrix} \text{vec } \underline{V} \\ &= \underline{\tilde{v}}_{nom} - \underline{J}_3 \quad \text{vec } \underline{V}\end{aligned} \tag{7.29}$$

which defines the matrix $\underline{J}_3$, while $\underline{\eta}$ is defined according to (6.4). Squaring (7.29) yields:

$$\underline{\tilde{v}}^T \underline{\tilde{v}} = \left\|\underline{\tilde{v}}_{nom}\right\|^2 - 2\,\underline{\tilde{v}}_{nom}{}^T \underline{J}_3 \text{ vec } \underline{V} + \left\|\underline{J}_3 \text{ vec } \underline{V}\right\|^2 \quad . \tag{7.30}$$

Let us take a closer look at the second term on the right hand side. First note that

$$\begin{aligned}\underline{\tilde{v}}_{nom}{}^T \underline{J}_3 &= \sum_{k=1}^{mR} v_{k\,nom}\left[\eta_{1_k}\underline{J}_2, \quad \eta_{2_k}\underline{J}_2, \quad \eta_{3_k}\underline{J}_2, \quad \ldots\right] \\ &= \sum_{k=1}^{mR}\left[v_{k\,nom}\eta_{1_k}\underline{J}_2, \quad v_{k\,nom}\eta_{2_k}\underline{J}_2, \quad v_{k\,nom}\eta_{3_k}\underline{J}_2, \quad \ldots\right] \quad ,\end{aligned} \tag{7.31}$$

where η_{ik} is the ith element of the trigonometric vector $\underline{\eta}$ at the kth time step. For the first term of $\underline{\eta}(\varphi)$ according to (6.4), one can derive:

$$\sum_{k=1}^{mR} v_{k\,nom}\ \eta_{1k} = \sum_{k=1}^{mR} v_{k\,nom} \cdot 1 \approx 0 \quad , \tag{7.32}$$

since, if the filter-hypothesis is correct, the innovations have zero mean. The other elements of $\underline{\eta}$ are harmonic functions whose values recur with each complete rotation. If we can assume ergodicity, i.e. if the statistical properties of the innovations do not depend on time, then the following holds for the other terms of $\underline{\eta}(\varphi)$, which "average" out due to the harmonic function and the zero-mean random variables:

$$\sum_{k=1}^{mR} v_{k_{nom}}\ \eta_{ik} = \sum_{j=1}^{m}\eta_{ij}\ \sum_{n=1}^{R} v_{(n-1)m+j_{nom}} \approx \sum_{j=1}^{m}\eta_{ij}\ \cdot 0 = 0 \quad . \tag{7.33}$$

Now, combining (7.30), (7.32) and (7.33), the variance of the innovations can be approximately written as:

$$S^2 = \frac{1}{mR}\left\|\underline{\tilde{v}}_{nom}\right\|^2 + \frac{1}{mR}\left(\text{vec } \underline{V}^T \underline{J}_3{}^T \underline{J}_3 \text{vec } \underline{V}\right) \quad . \tag{7.34}$$

The maximum variance occurs when vec $\underline{V}$ is the eigenvector of $\underline{J}_3{}^T \underline{J}_3$ whose corresponding eigenvalue is maximal:

$$S_{max}{}^2 = \frac{1}{mR}\left\|\underline{\tilde{v}}_{nom}\right\|^2 + \frac{1}{mR}\alpha_2{}^2 \max\left(\text{eig}\left(\underline{J}_3{}^T \underline{J}_3\right)\right) \quad . \tag{7.35}$$

The minimum variance occurs when vec $\underline{V}$ is the eigenvector of $\underline{J}_3{}^T \underline{J}_3$ whose corresponding eigenvalue is minimum. This minimum eigenvalue will be zero when $\underline{J}_3{}^T \underline{J}_3$ is rank deficient. In any case:

$$S_{min}{}^2 = \frac{1}{mR} \left\| \underline{\tilde{v}}_{nom} \right\|^2 + \frac{1}{mR} \alpha_2{}^2 \min\left(\text{eig}\left(\underline{J}_3{}^T \underline{J}_3 \right) \right) \quad . \tag{7.36}$$

We now calculate the robust reliability as in eqs. (7.26)-(7.28). Let $\left\| \underline{\tilde{v}}_{nom,1} \right\|^2$ and $\left\| \underline{\tilde{v}}_{nom,2} \right\|^2$ be the least and next-largest squared innovations. The analog of eq. (7.27) is

$$\left\| \underline{\tilde{v}}_{nom,1} \right\|^2 + \alpha_2{}^2 \max \text{eig}(\underline{J}_3{}^T \underline{J}_3) \quad \geq \quad \left\| \underline{\tilde{v}}_{nom,2} \right\|^2 + \alpha_2{}^2 \min \text{eig}(\underline{J}_3{}^T \underline{J}_3) \quad . \tag{7.37}$$

The least value of α_2 at which this relation holds is the robust reliability:

$$\breve{\alpha}_2 = \sqrt{\frac{\left\| \underline{\tilde{v}}_{nom,2} \right\|^2 - \left\| \underline{\tilde{v}}_{nom,1} \right\|^2}{\max \text{eig}\left(\underline{J}_3{}^T \underline{J}_3 \right) - \min \text{eig}\left(\underline{J}_3{}^T \underline{J}_3 \right)}} \quad . \tag{7.38}$$

8. Numerical Example: Reliability of the Crack Depth Estimate with respect to Sensor Deployment

Let us apply the robust reliability analysis to a simple rotor with a cracked shaft, modeled by eight finite beam elements. The dynamics underlying this particular example is also discussed in *Seibold (1995),* and *Seibold and Weinert (1996).*

The rotor is 1m long and 18mm in diameter, and modeled with 8 beam elements. A single transversal crack of depth 4mm is located between the 4th and 5th nodes. The shaft rotates with a constant frequency of 15.9 Hz. The first eigenfrequency for bending vibration of the rotor is 25 Hz. Fig.8.1 identifies the dofs of the finite element model. We will examine the variation of the reliability of the crack-depth estimate with the number and position of sensors. In this example, we are referring to the derivation in section 7.1.1, based on the ellipsoid-bound model of uncertainty.

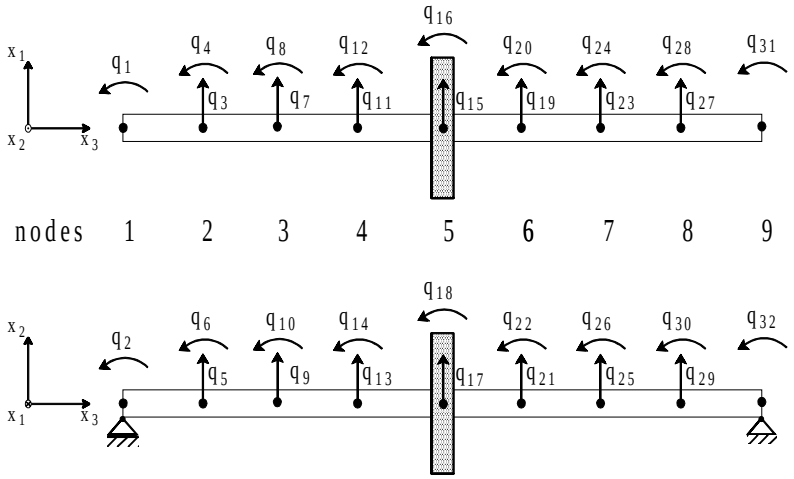

Figure 8.1: Finite element model of the rotor.

Eq.(7.11) shows that the robust reliability is a function of the sensor deployment matrix, $\underline{C}$, which appears in both the numerator and the denominator (see eqs. (7.6) and (7.7)). We will evaluate $\breve{\alpha}_1$ for different choices of $\underline{C}$, in order to compare the reliabilities of these alternative design options.

The different sensor deployments are numbered in the following way: deployment no. 1 uses four measurements of dofs 3, 5, 27 and 29. Deployments 2-12 each use these four and one additional measurement. For deployments no. 2-11 the additional measured dof is 7, 9, 11, ..., 25, respectively. For deployment no. 12 the additional measured dof is 16.

Eq.(7.11) shows that the robustness of the estimate depends on the angle of shaft-rotation, φ, at which the measurement is made. This angle-dependent reliability results from the rather complicated variation of the dynamic effect of the "breathing" crack. Fig. 8.2 is based on four sensors located near the supports of the rotor, two at each end, measuring horizontal and vertical displacements, dofs q_3, q_5, q_{27}, and q_{29}, in fig. 8.1. In this example we are investigating one rotation of the rotor, i.e. 360 time steps, and the crack depth estimate and Kalman gains have converged to within about 1%. The figure shows the angles at which the estimate is particularly robust with respect to the crack-shape uncertainty, at about 160 degrees and 280 degrees . Note that the crack opens at 0 degrees, and closes at 180 degrees. Figs. 8.3 and 8.4 show the variation with angle φ of the robustness for five sensors: the original four plus an additional sensor measuring horizontal displacement q_{15} (deployment no. 6), and vertical displacement q_{17} (deployment no. 7) respectively. Note that the maximum robustness does not occur at the same angle of rotation for deployments 1, 6 and 7.

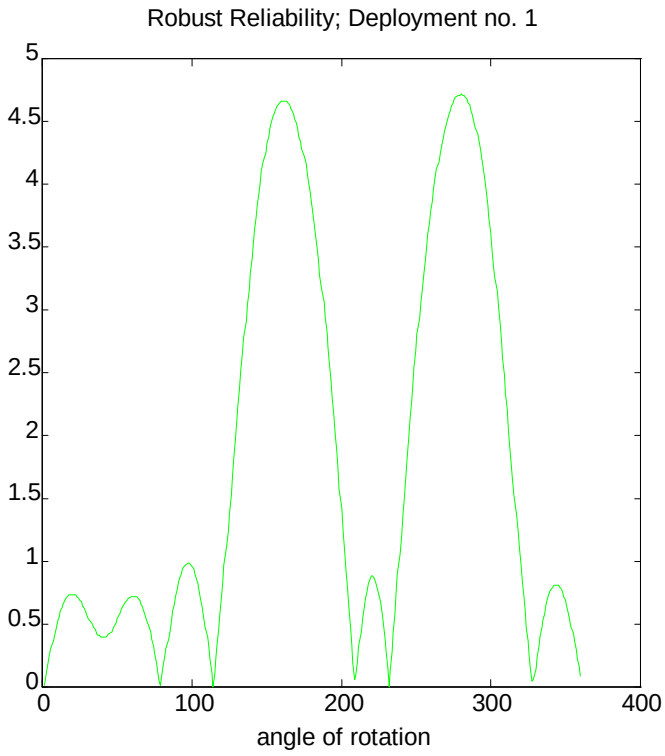

Figure 8.2: $\breve{\alpha}_1$ as a function of the angle φ for sensor deployment no. 1.

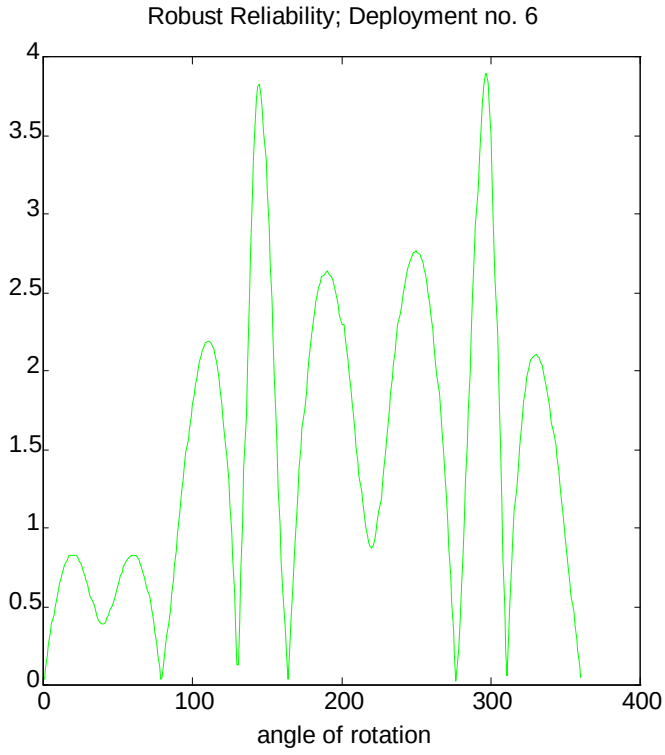

Figure 8.3: $\breve{\alpha}_1$ as a function of the angle φ for sensor deployment no. 6.

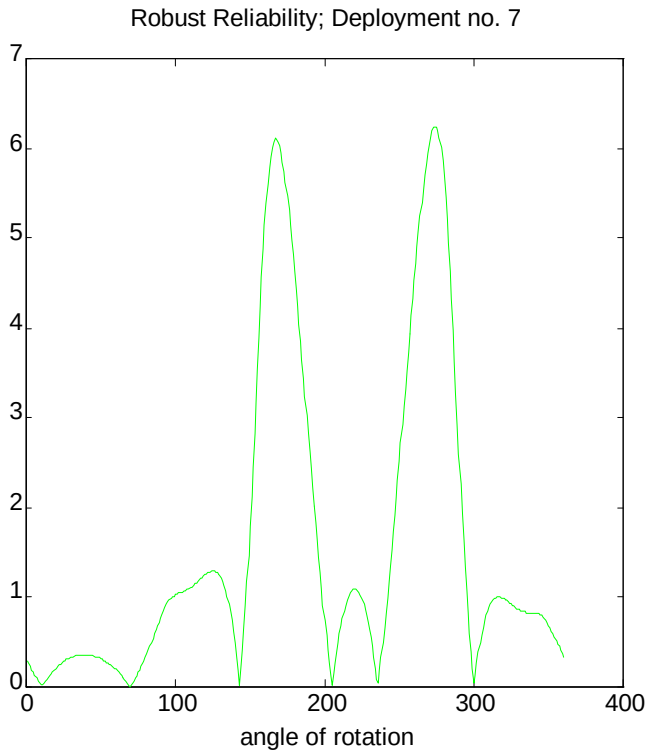

Figure 8.4: $\breve{\alpha}_1$ as a function of the angle φ for sensor deployment no. 7.

From now on we will only consider those angles at which the estimate is maximally robust.

In fig. 8.5, we see the maximal robustness for the 12 different sensor deployments described above. Deployment 1 is the four-sensor configuration represented in fig. 8.2. Each of the other configurations has these four plus one additional sensor. The additional sensor is moved progressively from near the support to the rotor midpoint. Deployment 6 is portrayed by fig. 8.3. In deployments 2, 4, 6, 8 and 10 the additional sensor measures a horizontal displacement, while in deployments 3, 5, 7, 9 and 11 a vertical displacement is measured by the additional sensor. In deployment 12 the 5th sensor measures a rotation at the rotor midpoint about the lateral horizontal axis, q_{16}.

In fig. 8.5, we note a weak tendency for improvement in reliability as the additional sensor is positioned nearer to the midpoint, where the displacements are greater and the crack-breathing is enhanced. Also, we note the strong preference for vertical over horizontal measurement. The physical reason is that only in the vertical direction, the two extreme states of the crack (fully open and fully closed) can be observed.

Fig. 8.6 shows the estimates of the crack depth for the different sensor deployments. The true value is 4 mm. It is interesting to note that deployment 12, i.e. the adding of an additional sensor measuring the rotations at dof no. 16, yields a rather bad estimate for the crack depth, even though the maximum robust reliability is relatively large in fig. 8.5. To make sense of this observation, one must define very precisely what we mean by $\breve{\alpha}$, the robust reliability: it is the greatest value of the uncertainty parameter α such that the **estimate** of the crack depth does not deviate from the nominal estimate by more than ε, eqs. (7.2), (7.11). By adding a sensor, we are adding both "information" and "noise", so the estimate will change; it may get better or worse; it may become more stable with respect to crack load uncertainty, it may not. The fact that $\breve{\alpha}$ is larger with an additional sensor does not mean that the nominal estimate itself is "correct". It does mean that variation around the nominal estimate is low.

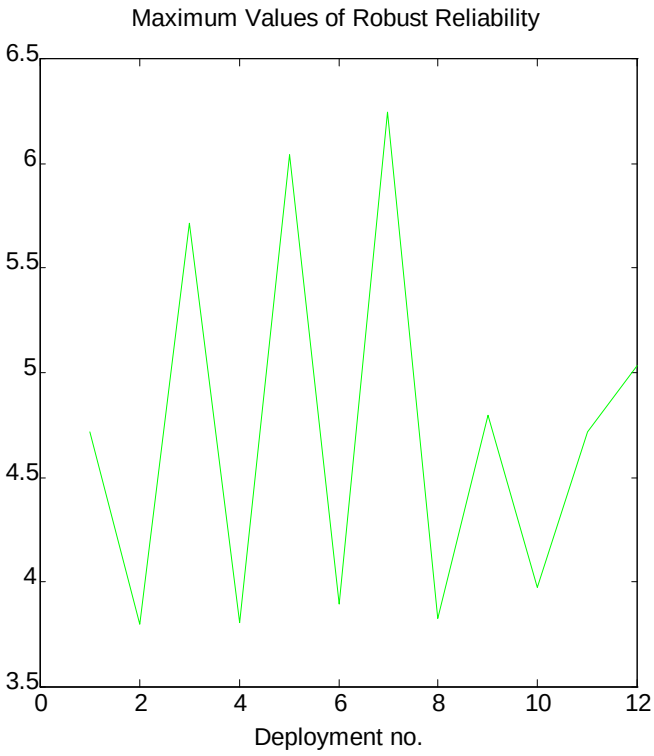

Figure 8.5: Maximum values of $\breve{\alpha}_1$ for the different sensor deployments.

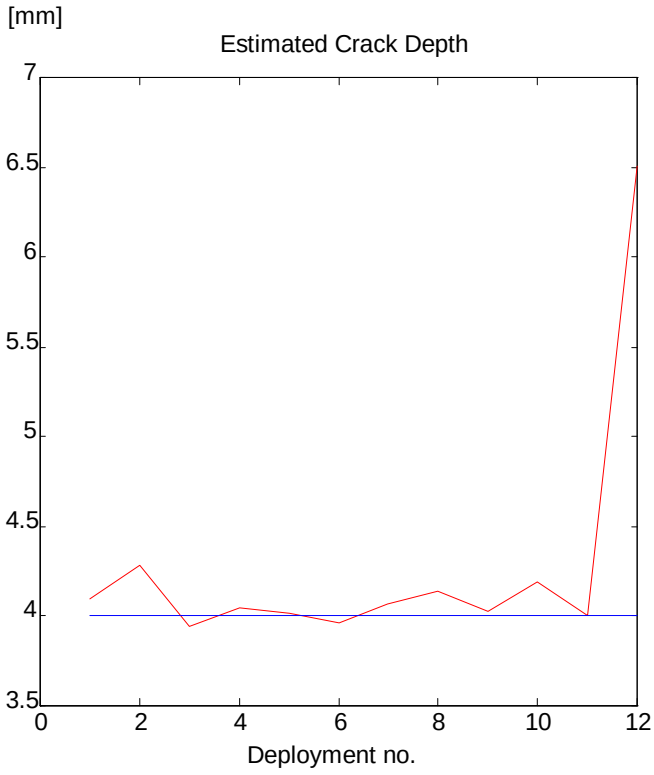

Figure 8.6: Estimated crack depths for the different sensor deployments.

An important factor which influences the robust reliability $\breve{\alpha}$ is the Kalman gain, eqs. (7.6), (7.11), or in other words the design of the filter. In fig 8.7, the variation of $\breve{\alpha}$ over one rotation for deployment 12 and different designs of the Kalman gain is displayed. It shows the results obtained with the original Kalman gain design and two new designs based on a increasingly larger covariance matrix $\underline{R}$, see eq. (5.7). It is obvious that the fluctuation of the curves decreases with increasing of $\underline{R}$, while the maximum value of $\breve{\alpha}$ does not change much. This means that in this example, the reliability is rather insensitive to the choice of the Kalman gain, provided that the filter has converged. In other cases one might observe sensitivity of the reliability to the filter design, in which case the reliability analysis is a means of choosing between alternative filters.

How can the reliability of the crack depth estimation be improved? First, it is very important to pick up enough samples per rotation, especially at the angles where the estimate is maximally robust. This seems to be a very simple point, but it is still customary e.g. in power plants to store only the maximum amplitude values, i.e. one sample per rotation. In this way, it is impossible to get enough measurement information about the complicated crack dynamics. Then, the design of the Kalman filter needs to be performed carefully. As has been stated above, the reliability analysis may be employed for choosing between different filter designs. Finally, the addition of one sensor will not always yield better results. It might well be worthwhile to investigate the "best" position for the respective circumstance.

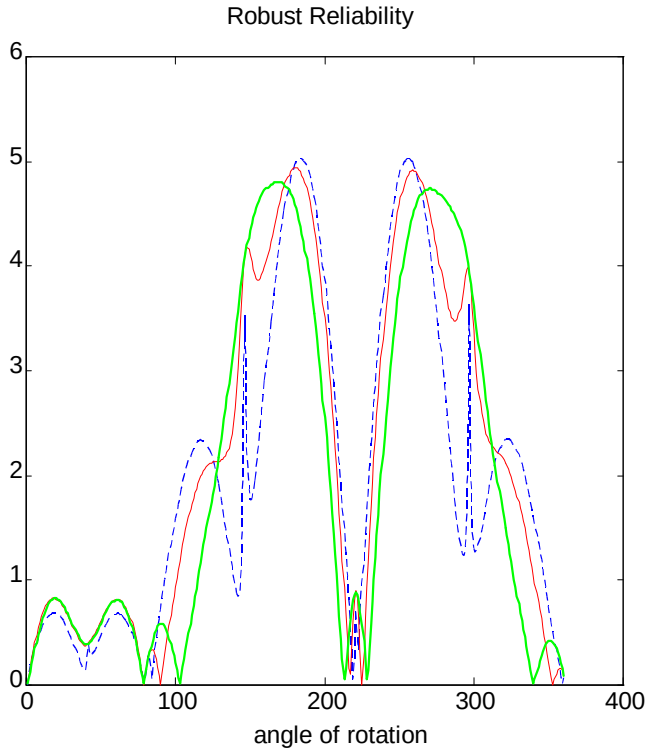

Figure 8.7: $\breve{\alpha}_1$ as a function of the angle φ for additionally measured rotation.
Sensor deployment no. 12 (---) and 2 new calculations with increasing covariance $\underline{R}$.

9. Calibration of Robust Reliability

We can compare different algorithm designs with the help of the robust reliability $\breve{\alpha}$. For instance, we can optimize the filter gains, or the number of parallel filters in the multi-hypothesis filter bank, or the number and location of the sensors. If $\breve{\alpha}$ is large, the algorithm is robust with respect to uncertainty, which is desirable. But, how large is large enough? To calibrate $\breve{\alpha}$, we have to establish a relation between $\breve{\alpha}$ and the safety of the algorithm. Of course, this leads in turn to the question: "How safe is safe enough?". The answer will always be based on subjective preferences. Still, such a relation is quite helpful to make sensible decisions.

Consider again the maximization of the robust reliability of the crack-depth estimate. Employing the ellipsoid-bound model of uncertainty, we obtained the robust reliability as a function of the measurement matrix $\underline{C}$, eqs. (7.6), (7.7) and (7.11):

$$\breve{\alpha}_1 = \frac{\left|\underline{K}_{ag}\,\underline{C}\,\underline{B}\,\underline{P}_1\gamma\right|}{\left\|\underline{K}_{ag}\,\underline{C}\,\underline{B}\right\|}\varepsilon_{CR} \quad . \tag{9.1}$$

As has already been stated in section 8, the reliability can be maximized with a suitable sensor deployment. For a given matrix $\underline{B}$, and a given number of sensors, the optimal sensor location can be calculated by varying $\underline{C}$ to maximize $\breve{\alpha}_1$. This may lead to the question how much better our results are if we employ more sensors. For such a decision, it will be helpful to consider the severity of the consequences of failure of the diagnostic algorithm, *Ben-Haim (1996)*.

Let us choose three different values for ε_{CR} in the failure criterion of eq. (7.2), corresponding to failure consequences of increasing severity:

$$\varepsilon_{CR1} < \varepsilon_{CR2} < \varepsilon_{CR3} \quad . \tag{9.2}$$

The most conservative failure criterion ε_{CR1} corresponds to low consequence severity, since failure is defined as occurring after only a very small error in the estimate. On the other hand, if we choose a large ε_{CR3}, we might anticipate catastrophic consequences as a result of failure of the diagnosis. In fact, one can imagine a continuum of failure criteria and plot the robust reliability as a function of ε_{CR} for one specific sensor deployment $\underline{C}_2$. Fig. 9.1 schematically shows the robust reliability of a particular deployment of sensors, $\underline{C}_2$, as a function of the severity of failure, ε_{CR}. Let us consider two more possible sensor deployments $\underline{C}_1$ and $\underline{C}_3$ and compare their reliabilities at medium severity, against deployment $\underline{C}_2$. We can see from fig. 9.1, that already for a moderate failure criterion, deployment $\underline{C}_1$ tolerates an amount of uncertainty which $\underline{C}_2$ can tolerate only by allowing high severity of failure. In other words, deployment $\underline{C}_1$ is, subjectively speaking, much more robust than deployment $\underline{C}_2$. Now consider sensor deployment $\underline{C}_3$. The figure shows that $\underline{C}_3$, also at medium consequence severity, can only tolerate a level of uncertainty which $\underline{C}_2$ tolerates at low severity. Thus $\underline{C}_3$ is "much" less robust than $\underline{C}_2$.

Depending on how much safety we require, we can now choose the appropriate sensor deployment. If high safety is needed, it might be worthwhile to choose sensor deployment $\underline{C}_1$, even if it may be more costly.

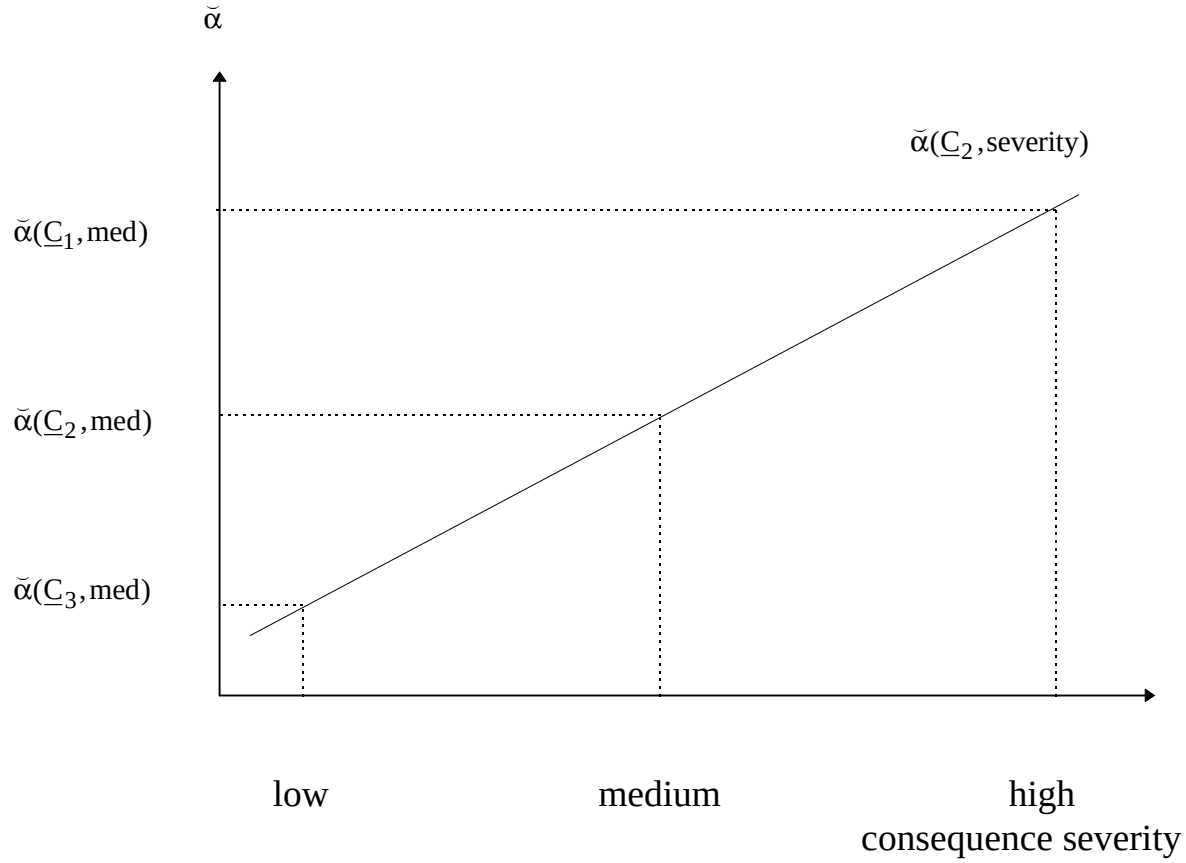

Figure 9.1: Robust reliability versus consequence severity:

10. Conclusion

In this paper, robust reliability of multi-hypothesis Kalman Filters concerning crack diagnosis in rotors was discussed. The question addressed was: how to optimize the multi-hypothesis algorithm with respect to the uncertainty of the spatial form and location of cracks and the resulting dynamic effects.

We have discussed the use of convex models in the context of a robust reliability analysis, and we have explained the design of a Kalman Filter for the diagnosis of cracks in rotors based on the crack model of *Theis (1990)*. We have formulated a measure of the robust reliability of the diagnostic algorithm, based on two different convex models of the uncertain crack loads depending on different prior knowledge. This measure is the robust reliability parameter $\breve{\alpha}$, which indicates the robustness with respect to uncertainties. We have explained a procedure for modifying the diagnostic algorithm for maximizing the reliability of the diagnosis. We have applied the analysis to the estimation of the depth of a crack, as well as to its localization. Finally, we have discussed the subjective calibration of the robust reliability parameter $\breve{\alpha}$.

11. Acknowledgment

This paper was written while one of the authors was on a research grant at the Technion-Israel Institute of Technology. The financial support of the DFG (Deutsche Forschungsgemeinschaft) under contract no. Se 578/5-1 is gratefully acknowledged. The authors are indebted to the S. Faust Research Fund at the Technion and to the Technion Fund for the Promotion of Research.

12. References

Ben-Haim, Y., 1985: *The Assay of Spatially Random Material,*
Kluwer, Holland.

Ben-Haim, Y., 1994: *Convex models of uncertainty: Applications and implications,*
Erkenntnis: An International Journal of Analytic Philosophy, 41, pp. 139 - 156.

Ben-Haim, Y., 1995: *A non-probabilistic measure of reliability of linear systems based on expansion of convex models,*
Structural Safety, 17, pp. 91 - 109.

Ben-Haim, Y., 1996: *Robust Reliability in the Mechanical Sciences,*
Springer, Berlin.

Ben-Haim, Y., 1997: *Robust reliability of structures,*
Advances in Applied Mechanics, vol.33, John Hutchinson, ed, pp.1--41.

Ben-Haim, Y., Elishakoff, I., 1990: *Convex Models of Uncertainty in Applied Mechanics,*
Elsevier, Amsterdam.

Frank, P.M., 1990: *Fault Diagnosis in Dynamic Systems Using Analytical and Knowledge-based redundancy - A Survey and Some New Results,*
Automatica, Vol. 26, No.3, pp. 459-474.

Gasch, R., 1976: *Dynamic Behaviour of Simple Rotors with a cross-sectional Crack,*
paper C168/76, I. Mech. E. Conf. Vibrations in Rotating Machinery, Cambridge, pp. 15-19.

Haas, H., 1977: *Großschäden durch Turbinen- oder Generatorläufer, entstanden im Bereich bis zur Schleuderdrehzahl,*
Der Maschinenschaden, 50, Heft 6, pp. 195-204. In German.

Isermann, R., 1984: *Process fault detection based on modelling and estimation methods,*
Automatica, 20, pp. 397-404.

Jazwinski, A.H., 1970: *Stochastic Processes and Filtering Theory,*
Academic Press, New York.

Kalman, R.E., 1960: *A new Approach to Linear Filtering and Prediction Problems,*
Trans. ASME, Series D, Journal of Basic Engineering, Vol. 82, pp. 35-45.

Lancaster, P., and Tismenetsky, M., 1985: *The Theory of Matrices,*
Academic Press, New York.

Mehra, R.K., Peschon, J., 1971: *An Innovations Approach to Fault Detection in Dynamic Systems,*
Automatica, 7, pp. 637-640.

Muszynka, A., 1992: *Vibrational Diagnostics of Rotating Machinery Malfunctions,*
Course on Rotor Dynamics and Vibration in Turbomachinery, von Karman Institute for Fluid Dynamics, Belgium.

Seibold, S., 1995: *Ein Beitrag zur modellgestützten Schadendiagnose bei rotierenden Maschinen,*
VDI-Fortschrittberichte, Reihe 11, Nr. 219, VDI-Verlag Düsseldorf. In German.

Seibold, S., Weinert, K., 1996: *A Time Domain Method for the Localization of Cracks in Rotors,*
Journal of Sound and Vibration, 195(1), pp. 57-73.

Theis, W., 1990: *Längs- und Torsionsschwingungen bei quer angerissenen Rotoren - Untersuchungen auf der Grundlage eines Rißmodells mit 6 Balkenfreiheitsgraden,*
VDI-Verlag, Düsseldorf, Reihe 11, Nr. 131. In German.

Wauer, J., 1990: *On the Dynamics of Cracked Rotors: A literature survey,*
Applied. Mechanics Review, vol. 43, no.1.

Williams, J.H., Davies, A., 1992: *System Condition Monitoring - An Overview,*
Noise and Vibration Worldwide, 23 (9), pp. 25-29.

Willsky, A.S., 1976: *A Survey of Design Methods for Failure Detection in Dynamic Systems,*
Automatica 12, pp. 601-611.

Abbreviations

EKF	Extended Kalman Filter

Nomenclature

$\underline{x}$	vector
$\underline{X}$	matrix
$\underline{X}^T$	transpose
$\hat{\underline{x}}$	estimated value of $\underline{x}$
$\|...\|_2$	Euclidean norm
vec($\underline{A}$)	vector formed by concatenating the columns of $\underline{A}$:

$$\mathrm{vec}(\underline{A}) = \mathrm{vec}\begin{bmatrix} A_{11} & A_{12} & . & A_{1n} \\ A_{21} & . & . & A_{2n} \\ . & . & . & . \\ A_{m1} & . & . & A_{mn} \end{bmatrix} = \begin{bmatrix} A_{11} \\ A_{12} \\ . \\ A_{1n} \\ A_{21} \\ . \\ A_{2n} \\ . \\ A_{m1} \\ . \\ A_{mn} \end{bmatrix}$$

$\underline{A} \otimes \underline{B}$	Kronecker product:

$$\underline{A} \otimes \underline{B} = \begin{bmatrix} A_{11}\underline{B} & A_{12}\underline{B} & . & A_{1n}\underline{B} \\ A_{21}\underline{B} & A_{22}\underline{B} & . & A_{2n}\underline{B} \\ . & . & . & . \\ A_{m1}\underline{B} & A_{m2}\underline{B} & . & A_{mn}\underline{B} \end{bmatrix}$$

a	crack depth
$\hat{a}_{nom}$	nominal crack depth estimate
$\underline{C}$	measurement matrix
$D(\alpha)$	set-theoretical convex model
$\underline{I}$	unity matrix
$\underline{F}_R$	vector of crack loads
$\underline{K}_g$	Kalman gain
$\underline{K}_{ag}$	bottom row of Kalman gain
$\underline{q}$	vector of global coordinates

$\underline{R}$	covariance matrix of measurement noise
S_i	standard deviation
$U(\alpha)$	set-theoretical convex model
$\underline{v}$	vector of innovations generated by a Kalman Filter
α	uncertainty parameter
$\breve{\alpha}$	robust reliability
ε	error of crack depth estimate
$\gamma(\varphi)$	vector of trigonometric functions
$\eta(\varphi)$	vector of trigonometric functions
φ	angle of rotation